Penerbit Akademia Baru

Journal of Advanced Research in Numerical Heat Transfer

Journal homepage:
http://www.akademiabaru.com/submit/index.php/arnht/index
ISSN: 2735-0142

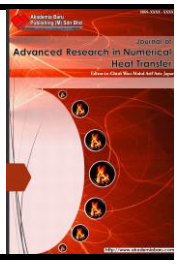

Numerical study and comparison of turbulent parameters of simple, triangular, and circular vortex generators equipped airfoil model

Ali Niknahad[1], Abdolamir Bak Khoshnevis[1,*]

[1] Department of mechanical engineering, Hakim Sabzevari University, Sabzevar, Khorasan Razavi, Iran

ABSTRACT

Drag force in long-haul flights can have a significant impact on fuel consumption. By modifying different parts of the aircraft structure, drag force and consequently fuel consumption can be significantly reduced. Vortex generators are tools that can delay and also weaken the separation phenomenon by creating vortices above the boundary layer, and the geometric shape of these tools can have a great impact on this. So far, the geometry of the vortex generators used on the Boeing 737 has been triangular. In this study, a comparison was made between circular and triangular vortex generators on the wing of Boeing-737 at 0 and 15 degrees of angle of attack by the means of numerical methods. Furthermore, the mean velocity and fluctuating velocity components in the wake region are numerically investigated in the wake region. Pressure drag, friction drag, total drag, and drag coefficient are considered and compared. Finally, a comparison is made between each model's lift to drag ratio. The results show a substantial decrease in the total drag by the use of a circular vortex generator. By attaching the vortex generators to the bare airfoil, the drag coefficient is reduced by 0.161% and 0.806% for triangular and circular vortex generators, respectively. The lift to drag ratio is increased by 3.54% and 3.65% for triangular and circular vortex generators, respectively.

Keywords:
Boeing-737; CFD; vortex generator;
fluctuation; drag reduction

Received: 6 October 2021 **Revised: 21 December 2021** **Accepted: 19 January 2022** **Published: 12 February 2022**

1. Introduction

Aerodynamic optimization has provided a suitable tool for all aerodynamic designs used in the design of aircraft, cars, trains, bridges, wind turbines, flow inside pipes, cavities, etc. Due to the issues of reducing fuel consumption and controlling the harmful effects on the environment, it is necessary to choose the best aerodynamic shape for different parts of the aircraft. CFD methods provide tools for the optimization of such configurations.

Khoshnevis *et al.,* [1] studied the effects of CFJ flow control on the aerodynamic performance of symmetric NACA airfoils. their study examined the sound effects of co-flow jet on the aerodynamic performance of some symmetric blade sectors of wind turbines. The aerodynamic coefficients alongside the lift to drag ratio were calculated and the consequences were compared together for the baseline and co-flow jet geometries. The outcomes of the baseline airfoils presented that the

* *Corresponding author.*
E-mail address: khoshnevis@hsu.ac.ir

NACA 0012 and NACA 0015 airfoils created a larger lift at small angles of attack where the NACA0018 andNACA0021 airfoils created a higher lift at higher angles of attack. Moreover, the found outcomes exposed that applying the co-flow jet has an affirmative result on suspending the stall angle and increasing the lift coefficient. The aerodynamic coefficients were more enhanced by increasing the thickness when the proper momentum coefficient was considered.

Fardimadan and Mokhtarzadeh [2] experimentally studied turbulence measures in the boundary layer as well as near-wake of an airfoil located upstream of a 90 degrees curve. They presented the results of an experimental investigation on the near-wake of a NACA 0012 airfoil located upstream of a 90 degrees curve section using hot-wire. Among the features studied were the properties of variations in the direction of the airfoil concerning the approaching flow and the properties of the freestream speed. Stress was employed on the boundary layer on the upper surface of the airfoil and the wake up to one chord interval downstream. The factors of attentiveness were the average and turbulence measures and their discrepancies in the streamwise, normal, and spanwise ways. Results of the study designated the sensitivity of the wake features to the boundary layers on the airfoil. Quantities of average speed and streamwise turbulence strength occupied in the spanwise way inside the wake naked wave-like differences.

Jir´asek [3] studied the vortex generator model and its application to flow control. He introduced a novel vortex-generator model, which offers an effective method for CFD computation of flow systems with vortex generators. The jBAY uses a new method for defining the model control points. By using this method, the model is simplified and performance and accuracy are improved. Simulation results by placing a vortex generator on a flat plate and using two control methods, an S-duct air intake and a high-lift wing configuration, have been provided. The results of the model show a very good agreement with both experimental and numerical simulation results. The results also show that this method is easy to use and can capture the details of the effects of the vortex generator in both internal and external flows.

Lei *et al.,* [4] enhanced the thermal-hydraulic act of a round pipe using stamped delta-winglet vortex generators. A novel round pipe with delta-winglet vortex generators was projected to advance the thermal-hydraulic act. The properties of AOA of VG on heat transfer and fluid flow were inspected in depth. The consequences proved that delta-winglet vortex generators produce whirling movement of the stream to improve the stream involvement in the round pipe causing heat transfer intensification with a reasonable pressure drop. It was established that the Nu number rises with the growing AOA and decreasing pitch of the VG.

Lemenand *et al.,* [5] studied vorticity and convective heat transmission downstream of a vortex generator. It contained a rudimentary formation with an exclusive vorticity generator implanted on the footwall of a heated straightforward passage. The goal of this effort was to examine the extent that the convective heat transmission is connected to the vorticity. It was revealed that there is a robust association between the vorticity flux and Nu number near to the vortex generator, although the axial difference deviates for measures when going downstream. The Nu number shows a severe top over the VG and falls close to its rudimentary level behindhand the VG.

Narasimhan *et al.,* [6] forecasted wake in a bent duct. In their study, empirical information on the growth of an airfoil wake in a bent stream was compared with computation founded on the k-$\boldsymbol{\varepsilon}$ model. The average speed shape was unbalanced, the half-width of the wake was further on the internal side of the bent duct than on the outward, and the turbulent shear stress fell quickly on the outward. The standard k-$\boldsymbol{\varepsilon}$ model was capable of adequately replicating these actions. Creating C_{μ}, reliant on the local radius advanced the correspondence on the inward side but somewhat deteriorated it on the outward.

Okamoto *et al.*, [7] studied active communication of the lengthwise whirlwinds by active vortex generators. Their study emphasizes active communication brought in the period be an average of features of the lengthwise whirlwinds downstream of a couple of active whirlwind generators with numerous kinds of whirlwind configuration. It was essential to comprehend the occasionally acted interrelating procedures among the turbulent boundary layer and the lengthwise whirlwinds. The aim was to explain empirically the period be an average of distinguishing velocity and the whirlwinds, and to argue whirlwind development linked with the stable whirlwinds by the firm whirlwind producers.

Szwaba *et al.,* [8] studied current-wise vortex production by the pole. In the case of using a jet vortex generator, a current wise vortex was announced by a tilted jet. It had been suggested to put out a pole in its place of a jet. It had been revealed that the use of a pole can present an identical consequence as a jet. The consequences accessible in these empirical and computational inquiries deliver rules for the intention of a novel technique enthusiastic chiefly to exterior currents.

Tulapurkara [9] studied turbulence models for the calculation of flow preceding aircraft. The subject of turbulence models for the calculation of flow preceding aircrafts had not the acceptable devotion as was expected. The Reynolds averaged equations for compressible viscous flow were defined and the necessity for turbulence modeling was emphasized in this appraisal. To measure the appropriateness of a turbulence model, the calculations brought in it should be likened with consistent empirical data. Henceforth, a short-lived debate on accessible standard information concerning aircraft apparatuses was offered. Calculations using these models and the consequences were labeled in this evaluation. It seemed that the Baldwin and Lomax model is appropriate for the calculation of attached flows. Also, with adjustment recommended by Degani and Schiff, this model provides decent consequences for flows from place to place of bulks with crossflow separation. The Johnson and King model was proposed to provide judicious consequences even for flow separation. Two-equation models, algebraic models, and RSM were also investigated.

Tajuddin *et al.,* [10] studied flow characteristics of a blunt-edged delta wing at a high angle of attack. In their work, the chief objective is to study the flow characteristics of the VFE-2 blunt-edged delta wing profiles at a high angle of attack. The vortex is advanced on the upper surface of the delta wing and this physics of flow is very complex. The vortex flow on the sharp-edged wing advances in the Apex region. some flow topology is detected for the blunt-edge wing. In the apex region, the vortex on the blunt-edged wing is not advanced but at a cord-wise position based on AOA, Re, and leading-edge bluntness. The primary vortex progressed upstream with increasing AOA. The problem is that this vortex will be made to the apex if the AOA is more enlarged. The tuft method was also done to visualize the flow features overhead the surface of the delta wing at high AOA. The consequences acme flow physics overhead blunt-edged wing at high AOA. The consequence displays that the primary travels upstream closed the apex at high AOA.

Adanta *et al.,* [11] studied the performance comparison of NACA 6509 and 6712 on pico hydro type cross-flow turbine by numerical method. In their study, they examined the use of airfoils for cross-flow turbine blades to conclude whether lift force can increase performance. Using CFD, their study compares NACA blades 6509 and 6712. The maximum mechanical efficiencies of the turbine when using NACA blades 6509 (47.6%) and 6712 (46.9%) are less proficient than standard blades at 77.8%. the first reason is satisfactory lift force is not created by airfoil blades. The second reason is that rotation and torque cut in stage 2 by means of pressure cut at the bottom of the blade and the final reason is that energy absorption in stage 2 is not optimal due to the internal impeller occurrence of flow recirculation or vortex. By using standard blade shape, minimizing flow recirculation or vortex,

and designing the runner based on the ratio between turbine tangential velocity and water tangential velocity of 1.8 or the ratio of turbine velocity and inlet velocity of 0.53, the turbine can be optimized.

Adanta *et al.,* [12] studied the assessment of turbulence modeling for numerical simulations into pico hydro turbine. Currently, the computational fluids dynamics (CFD) method is becoming an important subject of research in engineering, and pico hydro seems to be of particular interest. To increase accuracy using the CFD method, the assumptions made should be close to the actual conditions. However, there has been no comprehensive study that explains the characteristics and turbulent models that are considered suitable for use in the pico hydro turbine. their study aims to explain flow characteristics to determine whether turbulent flow would occur and recommends a turbulent model that may be applied to a pico hydro turbine. To achieve the objectives of the study, several methods are used, including asymptotic invariance (Reynolds number analysis), local invariance, theoretical analysis, and a literature study. their study found that the flow profile that occurs is irregular; the Reynolds number flow is 420,972, within the turbulent flow category; vorticity occurs with the prediction using isotropic assumptions; flow dissipation occurs, and is continuous because turbulent kinetic energy is supplied from the main flow. Thus, the category of water flow in a pico hydro turbine with a power potential of 1 kW is turbulent. The literature study reveals that the prediction of turbulent flow in the pico hydro turbine can be realized by three models: standard k-ε is recommended for the overshot waterwheel, RNG k-ε is recommended for the undershot waterwheel and cross-flow turbine, SST k-ω is recommended for propeller or open flume, Pelton, breastshot waterwheel and Turgo turbines. However, these recommendations do not constitute a conclusion because a good turbulent model is based on actual conditions.

Abdul Hakim *et al.,* [13] investigated the effects of Reynolds number on flow separation of Naca airfoil. The objective of their study is to examine the flow separation overhead UTM 2D Airfoil at three dissimilar Reynolds numbers using pressure distribution technique and flow visualization. On three different wingspans,40%, 50%, and 70%m of span, the pressure distribution was measured and plotted to understand the flow features at AOA from 0° to 35°. The flow visualization technique was completed from 0° to 18°. It is concluded that flow in the Reynolds number of 1×10^6separates at 16°; in Reynolds number of 1.5×10^6 separates at 18° and in Reynolds number of 2×10^6 separates at 20°.

Fahmi Mohd Sajali *et al.,* [14] simulated the effect of various distances between the front and rear body on the drag of a non-circular cylinder. The non-circular cylinder front surface for a positive pressure of the unsteady vortex generation, the square plate was attached upstream of the cylinder. The streamlines that separate from its edges are modified to attach smoothly onto the front face shoulders of the main body. The consequence of this modification results in minimum drag. The consequences specify that the sideways faces and the back faces have low pressure. The pressure drag coefficient can be a value in the range of 1.0 - 1.42.

Eleiwi *et al.,* [15] numerically studied fluid flow and heat transfer in a backward-facing step with three adiabatic circular cylinders. In their work, the examination of the heat transmission improvement and fluid flow features of three adiabatic cylinders in the backward-facing steps are done by CFD. The effects of RE, heat fluxes, and space between two successive cylinders on the heat transfer features are investigated. the consequences demonstrate the heat transmission is augmented. The reattachment space is reduced when using cylinders. The heat transmission improvement grows from 6 % to 13 % if the Re changes from 50 to 250 when heat flux increases 67%.

Cerutti *et al.,* [16] performed a flow field analysis for aerodynamic drag reduction employing platooning configurations of light commercial vehicles. Platooning formations of two, three, and four vehicles were tested. planar PIV measurements were executed to examine the near wake of the two-

vehicles platoon shape. 30% and 43% of drag reductions were demonstrated for the front and the rear vehicle for the two-models platoon. at an inter-vehicle distance, drag reduction is about 36.5%. the benefit associated with the platooning configuration reduces by increasing distance. the vehicle's drag to the flow field organization and the modal energy distribution are related. the main component that is accountable for the wake introduction is the large vortex created near the upper edge of the vehicle's base. the slant angle doesn't affect the drag decline of the leading vehicle, while it is able to lead to greater changes in the case of the rear vehicle. greater values of the drag decline are observed for three and four-vehicle platoons.

Li *et al.,* [17] studied Vortex generator design and numerical investigation for wake non-uniformity and cavitation fluctuation pressure reduction. in their paper, a vortex generator is mounted on the outward of ship stern to increase the quality of ship wake and resolve the shaking problem. the dimensions and mounting location of the vortex generator are planned based on the vessel body lines. the numerical computation is done for the simple hull and hull with a propeller vortex generator system to examine the efficiency of the vortex generator. By mounting the vortex generator, the wake alterations mostly happen in the district close to 12 o'clock. The speed in the high wake zone gains acceleration and the edge transition of wake develops more moderate which results in a smooth transition of the blade unsteady cavitation in edge track. the alterations of wake can postpone the edge angle of the blade cavitation failure. It grows the space between the locations where the blade cavitation collapsed and the vessel foot casing. It can also cut the largeness of fluctuating pressure.

Ricco *et al.,* [18] reviewed turbulent skin-friction drag reduction by near-wall transverse forcing. In their research, the most operative technique of doing so is declared as using active control on the near-wall layer by exposing the drag-crating flow in the boundary layer to a transient and/or locally variable cross-flow component. Drag can be reduced by 50% by using this. their review includes experimentations, simulation, analysis, and modeling for boundary layer and channel flow. Their work includes subjects such as the drag-reduction boundary, the primary physical occurrences that donate to the clarification of the source of the drag discount, the dependency of the drag discount on the Re, inactive control techniques, and consideration of possible forthcoming study and applied comprehensions.

Nagler [19] studied Boeing 737 – 300 wing aerodynamics calculations based on VLM theory. aerodynamics factors of Boeing 737 - 300 are computed employing vortex lattice method theory. The wing was separated into pieces of the 6X6 dimensions. The wing was supposed to be planar and the pieces are in the trapezoid figure. Aerodynamics lifting and moment factors and center of pressure were computed. The maximum lifting factor inaccuracy between previous works and VLM is around 4.0% and between finite wing theory is about 2.2%. the error of center of pressure location between FWT and VLM is around 0.5%.

J. KC *et al.,* [20] investigated experimentally conformal vortex generators via wake survey. Their work demonstrated the investigation of conformal vortex generators with wake surveys in a wind tunnel. Several conformal vortex generators formations were applied independently to a LA203A wing model. The conformal vortex generators can generate robust coherent structures that continued into the wake. Making the conformal vortex generator dimensions lesser faded the coherent constructions. the coefficient of drag was higher at high angles of attack when the step of conformal vortex generators moved further upstream. conformal vortex generators can perform better than a backward-facing step.

Increasing the lift-to-drag ratio, reducing drag force, and consequently reducing fuel consumption can be achieved by using newer vortex generators that have the ability to create stronger vortices on

the boundary layer. What is clear is that the vortex generators used on the Boeing 737 have all been triangular in nature and no different geometries have been used. The importance of the present article is that a new model of generator vortex has been introduced that has the ability to create stronger vortices on the boundary layer formed on the wing of the aircraft and can reduce the drag force in a favorable way. Accordingly, airlines will be able to drastically reduce their fuel costs for short-haul and long-haul flights by changing the shape of their Boeing-737 vortex generators. In this study, by using CFD methods and implementing RSM for turbulence modeling, flow fields consisting of mean velocity and Reynolds stress around three separate airfoils, simple, equipped with a triangular vortex generator, and equipped with circular vortex generator of Boeing-737, are computed at 0 and 15 degrees stall angle of attack [23]. The graphs of mean velocity, velocity defect, and Reynolds stress are sketched for comparison according to each airfoil case. The changes in these values are also reported. Finally, by making a comparison between the amount of drag reduction and the increase of lift to drag ratio, the suitable shape of the vortex generator is determined

2. Methodology

2.1. Governing Equations

The results obtained in the present paper are obtained by solving the continuity and Navier-Stokes equations for incompressible flow. The incompressibility condition is true since the Mach number of the stream in this study is less than 0.3. Eqs. (1)-(2) show the RANS equitation for continuity and momentum in the X-direction.

$$\frac{\partial \bar{u}}{\partial x}+\frac{\partial \bar{v}}{\partial y}=0 \tag{1}$$

$$\bar{u}\frac{\partial \bar{u}}{\partial x}+\bar{v}\frac{\partial \bar{u}}{\partial y}+\frac{1}{\rho}\frac{\partial \bar{p}}{\partial x}=\nu(\nabla^2\bar{u})-\frac{\partial \overline{(u')^2}}{\partial x}-\frac{\partial \overline{(u'v')}}{\partial x} \tag{2}$$

Where $\bar{u}, \bar{v}, \rho, \bar{p}, \nu, u'$ and v' are X-dir average velocity component, Y-dir average velocity component, density, kinematic viscosity, X-dir velocity fluctuation component, and Y-dir velocity fluctuation component, respectively.

Also, To model the turbulent flow in the present study, RSM has been used, which instead of high computational time, provides accurate answers. Eq. (3) to Eq. (12) illustrate this method. RSM relies on the "Reynolds Stress Transport Equation". The equation for the transport of kinematic Reynolds stress $R_{ij}=\langle u_i' u_j' \rangle$ is:

$$\frac{DR_{ij}}{Dt}=D_{ij}+P_{ij}+\Pi_{ij}+\Omega_{ij}-\varepsilon_{ij} \tag{3}$$

Where $D, P, \Pi, \Omega, \text{and } \varepsilon$ are diffusion term, production term, pressure-strain correlation term, rotational term, and dissipation term, respectively.

The description of each term is presented as follows:

Production term:

$$P_{ij}=-\left(R_{im}\frac{\partial u_j}{\partial x_m}\right)+R_{im}\frac{\partial u_i}{\partial x_m} \tag{4}$$

Rapid pressure-strain correlation term:

$$\frac{\Pi_{ij}^{R}}{k} = C_2 S_{ij} + C_3\left(b_{ik}S_{jk} + b_{jk}S_{ik} - \frac{2}{3}b_{mn}S_{mn}\delta_{ij}\right) + C_4(b_{ik}W_{jk} + b_{jk} + W_{ik}) \quad (5)$$

$$b_{ij} = \frac{\overline{u_i u_j}}{2k} - \frac{\delta_{ij}}{3} \quad (6)$$

Where $\Pi^R, k, C_{2,3,4}, S, b, \delta, W$ are rapid pressure-strain correlation term, turbulent kinetic energy, rapid pressure strain correlation model coefficient, rate of strain, Reynolds stress anisotropy tensor, Kronecker delta, and rate of rotation, respectively.

Slow pressure-strain correlation term:

$$\Pi_{ij}^{S} = -C_1\frac{\varepsilon}{k}\left(R_{ij} - \frac{2}{3}k\delta_{ij}\right) - C_2\left(P_{ij} - \frac{2}{3}P\delta_{ij}\right) \quad (7)$$

Where Π^S and C_1 are slow pressure-strain correlation term and slow pressure strain correlation model coefficient, respectively.

Dissipation term:

$$\varepsilon_{ij} = \frac{2}{3}\varepsilon\delta_{ij} \; or \; e_{ij} = 0 \quad (8)$$

$$e_{ij} = \frac{\varepsilon_{ij}}{\varepsilon} - \frac{2\delta_{ij}}{3} \quad (9)$$

Where e is dissipation rate anisotropy.

Diffusion term:

$$D_{ij} = \frac{\partial}{\partial x_m}\left(\frac{v_t}{\sigma_k}\frac{\partial R_{ij}}{\partial x_m}\right) = div\left(\frac{v_t}{\sigma_k}\nabla(R_{ij})\right) \quad (10)$$

$$v_t = C_\mu\frac{k^2}{\varepsilon}, \sigma_k = 1, C_\mu = 0.090 \quad (11)$$

Where v_t is turbulent kinematic viscosity and σ and C_μ together are diffusion coefficients.

Rotational term:

$$\Omega_{ij} = -2\omega_k\left(R_{jm}e_{ikm} + R_{im}e_{jkm}\right) \quad (12)$$

Where Ω and ω are rotational term and rotation vector, respectively. $e_{jkm} = 1$, if i, j, k are in cyclic order and are different. $e_{jkm} = -1$, if i, j, k are in anti-cyclic order and are different. $e_{jkm} = 0$ in case any two indices are the same.

2.2. Computational Domain

In this study, triangular and circular vortex generators equipped with airfoils of Boeing 737 and also simple airfoil without any vortex generator are considered. The chord line is 200 mm and the thickness is 20mm [21]. For modeling the vortex generator, the value 0.023 is selected for the ratio

h/c ratio, where “h” and “c” are vorticity generator (tab) height and chord length. Furthermore, the value 3 is selected for the ratio l/h. So the height and length of the vortex generator are 5 and 15 mm, respectively. The diameter of the circular vortex generator is also15mm. The vortex generators are installed in x/c=0.450 position on the top surface of the wing [22]. Figure 1 shows the Boeing-737 airfoil with and without vortex generators.

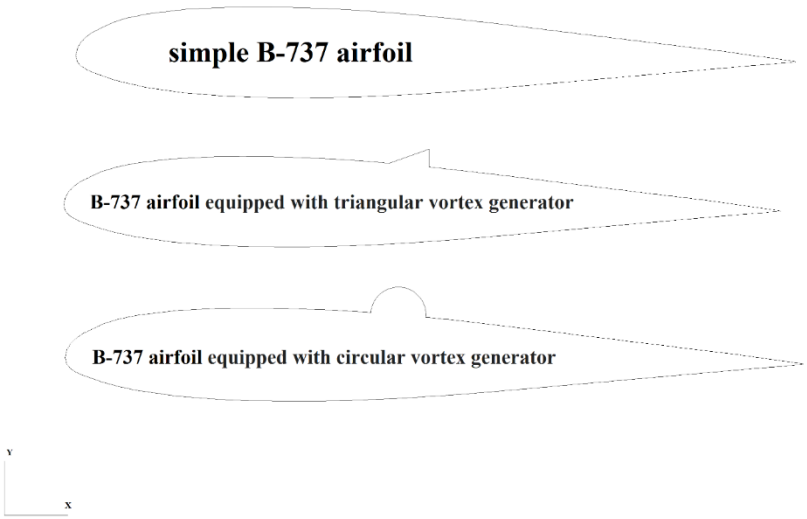

(a)

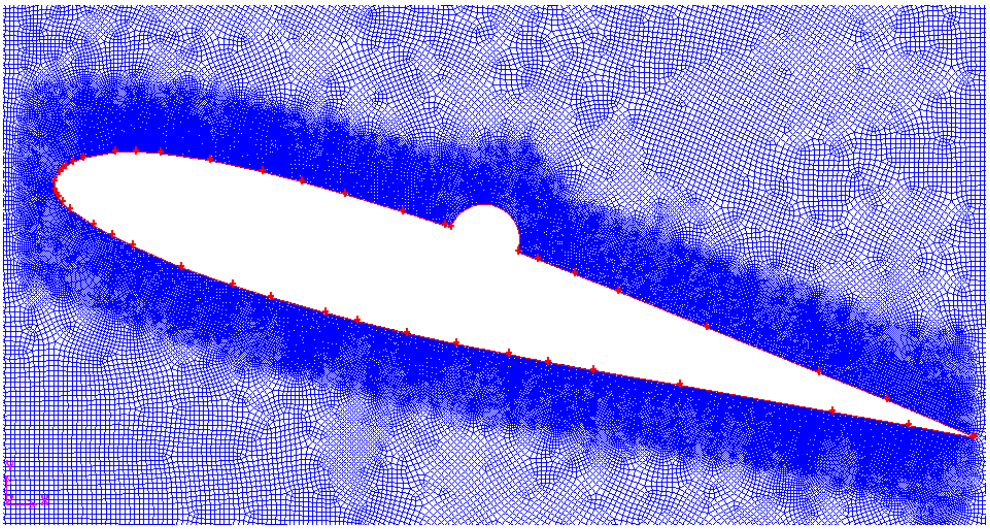

(b)

Fig. 1. The schematic of Boeing-737 with and without vortex generator(a), depiction of mesh grid(b)

2.3. Mesh Independency and Simulation Parameters

The computational grid contains 2700000 cells as an appropriate mesh number to achieve the mesh independency limit. Table 1 demonstrates the alteration of maximum velocity and drag coefficient according to three cases.

Table 1
Mesh independency limit

Cell number	Maximum velocity(m/s)	Drag coefficient	Error(%)
1800000	23.996	0.966	-
2700000	24.425	0.983	1.756
4050000	24.427	0.983	0.008

The equations are solved by using FLUENT 6.3.26. In the present study, the solver is steady and pressure-based. Velocity-pressure coupling is SIMPLE and pressure and velocity are discretized using standard and first-order upwind methods. The freestream turbulent intensity is set to 0.1%. The Reynolds number based on chord length is 1.6×105. Density and viscosity of air are considered as 1.225 kg/m3 and 1.7894e-05 kg/m-s, respectively. Table 2 shows the boundary conditions.

Table 2
Boundary conditions

Zone	Type	Velocity(m/s)	Pressure(atm)	Turbulent intensity(%)
Inlet	Velocity inlet	10 (m/s)	-	0.1
Outlet	Pressure outlet	-	1	0.1
Airfoil	Wall	No-Slip	-	-

3. Results and discussion

3.1. Validation

To validate and evaluate the accuracy of the present study, the profiles resulting from the passage of flow through the vortex generators in experimental studies have been compared with the results of numerical simulations. A vertical vortex generator (Figure 2) is compared by DNS and RSM results [5]. The flow configuration consists of a square duct flow of 7.620 cm for each side and its length is equal to 33.150 mm. vorticity generator of trapezoidal shape is installed on the bottom wall with an inclination angle of 24.5° relative to the wall plane. The leading edge of the vorticity generator is located at z = 13 cm. The dimensions of the physical domain and the vorticity generator are schematically shown in Figure 2. In the following sections, all spatial scales are scaled with the tab height h = 0.300 cm. The vortex generator thickness is 0.500 mm.

In this case, the free stream velocity is 0.160 m/s which corresponds to Reynolds number 12100 based on channel height. Figure 3 shows the y component of mean velocity divided by total free stream velocity versus non-denominational height. Figure 3 also shows the comparison between the DNS [5] and RSM. Although the RSM method is more time and cost-efficient than DNS, the agreement is well.

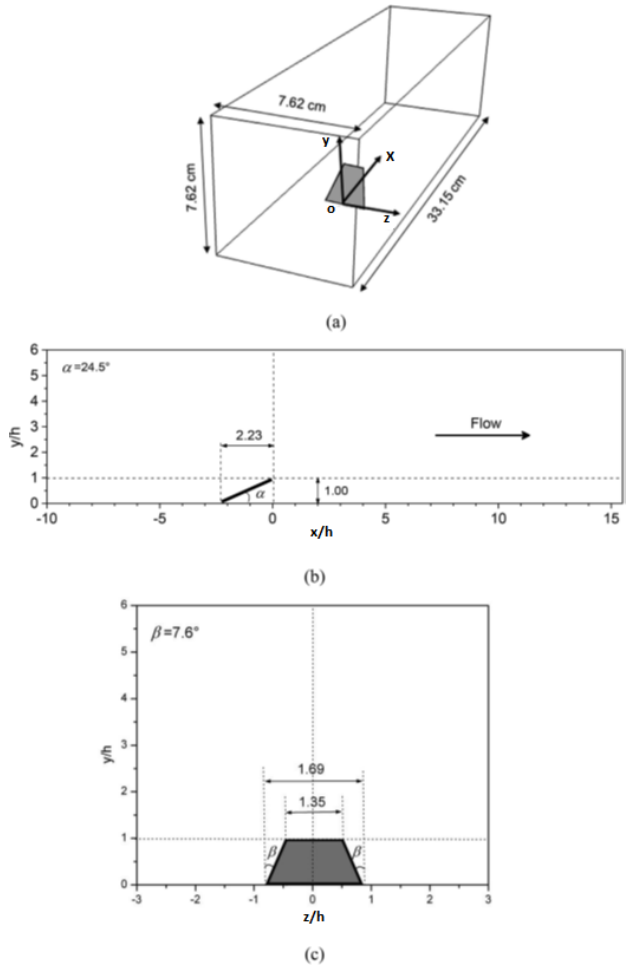

Fig. 2. Schematic of vortex geometry used for validation [5]

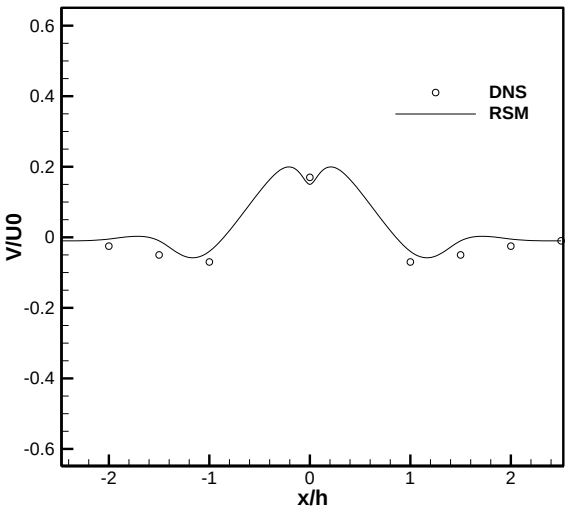

Fig. 3. comparison of V/U0 around vortex generator obtained by RSM and DNS [5] method

3.2 Reynolds Stress

In this section, the fluctuating velocity is obtained by the numerical RSM method. Figure 4 shows the non-dimensionalized $\sqrt{\overline{u'^2}}$ by free stream velocity versus Y/C for each station. The RSM method clearly shows the twin peaks at every station. The fluctuating velocity graphs show that by getting farther from the trailing edge of the airfoil the wake becomes weaker and weaker and turns into symmetry. By further inspecting and noting that the airfoil of Boeing 737 cross-sectional airfoil is asymmetric, it is found that the fluctuating velocity peaks are asymmetric too. Due to the existence of the camber, the upper fluctuating peak (right peak) is higher at several stations behind the trailing edge. The airfoil with a vortex generator produces higher vorticities than a simple one. The reason is the presence of large vorticities on top of the airfoil that produces the strong vorticities behind the airfoil. The results also show that the vorticities of a circular vortex generator are stronger than the triangular vortex generator, due to the separation of flow on a circular vortex generator. Figures 5 and 6 also show the wakes and vorticities behind vortex generators. In Figure 5 the existence of large vorticities behind the circular vortex generator is clear and these extensive wakes are responsible for significant drag reduction of the airfoil. Figure 5 shows that the wake of a circular vortex generator extends to 37.500% more than the triangular vortex generator wake. Table 3 shows the comparison of average peaks fluctuation of triangular/circular vortex generators equipped with airfoils with the simple one. The results show that at satiation X/C:0.050 and 0.100 the Reynolds stress produced by the circular vortex generator is stronger than the triangular vortex generator for the left peak but the results are vice versa at the remaining stations. Also, the results show an enormous increase in fluctuation velocity compared with simple airfoil wake. These fluctuations have a direct effect on suspending the separation and finally reducing pressure drag.

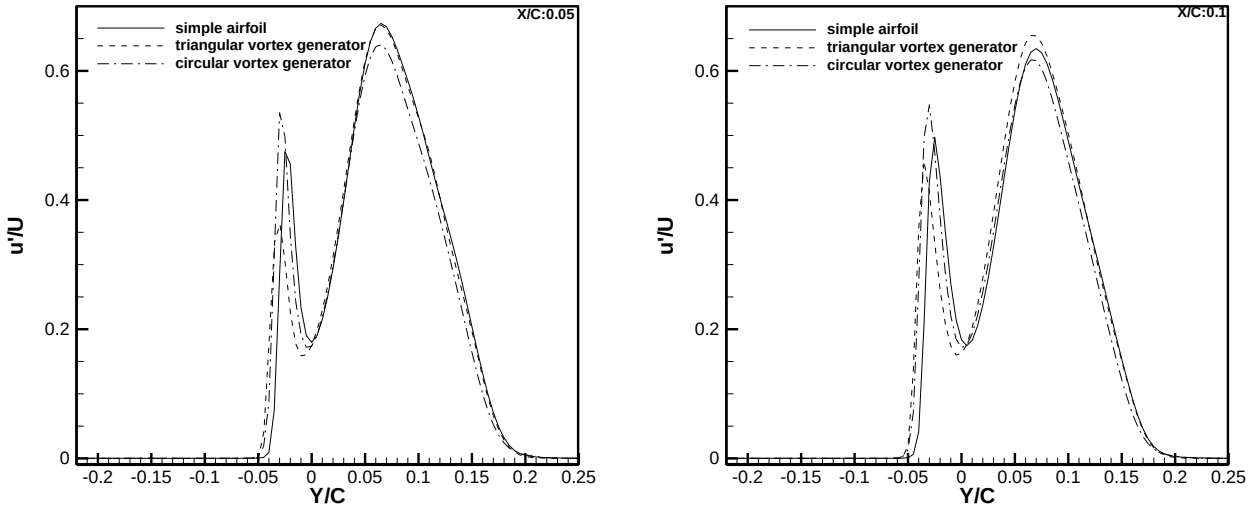

(a) (b)

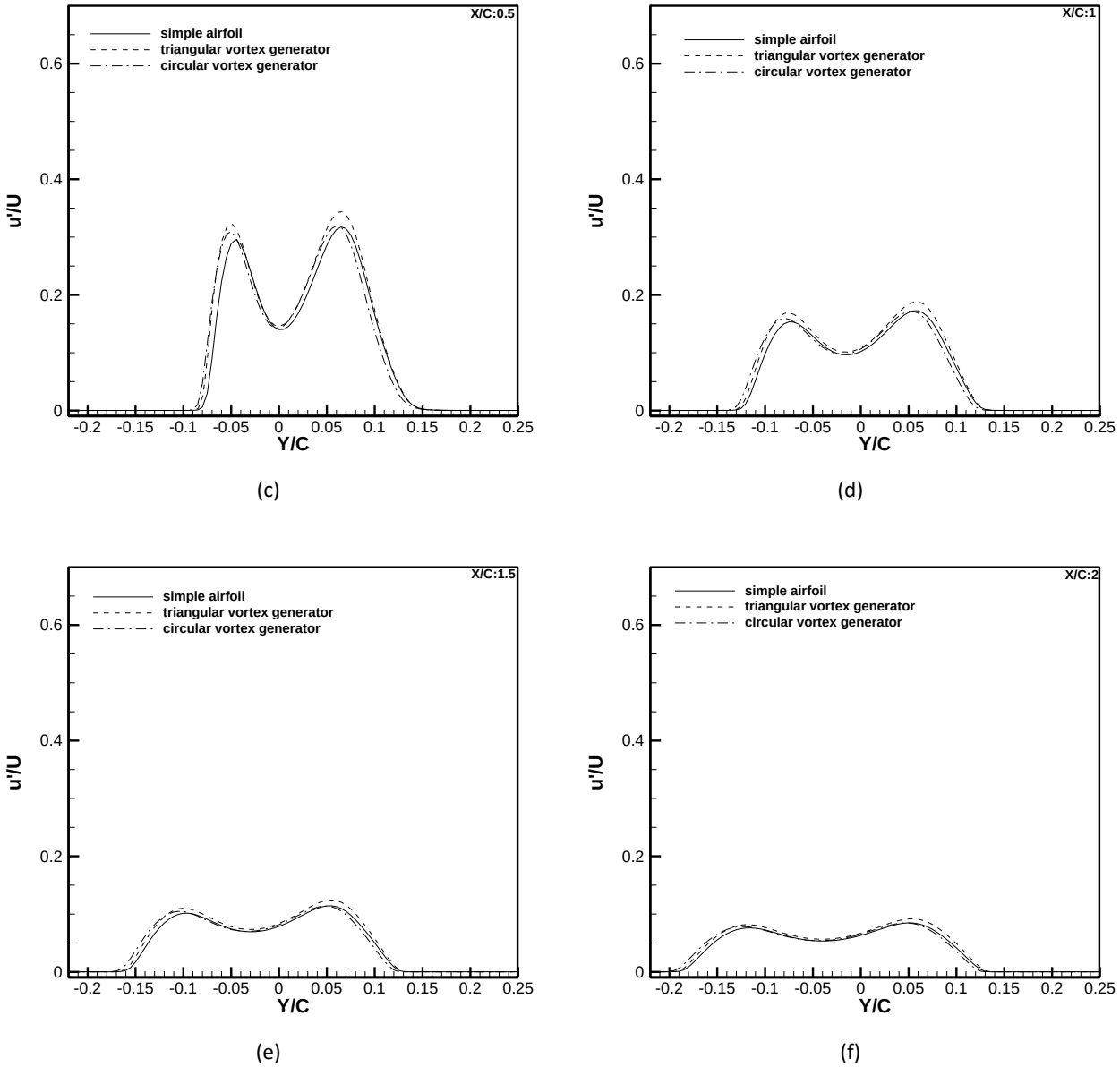

Fig. 4. The comparison of non-demintional Reynolds stress by RSM at stations X/C=0.05(a), 0.1(b), 0.5(c), 1(d), 1.5(e), 2(f)

Table 3
Comparison of averaged simple and triangular/circular vortex generators peak values

X/C	Average of peaks of an airfoil with triangular vortex generator($\frac{\sqrt{\overline{u'^2}}}{U}$)	Percent of increase(%)	Average of peaks of an airfoil with circular vortex generator($\frac{\sqrt{\overline{u'^2}}}{U}$)	Average of twin peak of the simple airfoil($\frac{\sqrt{\overline{u'^2}}}{U}$)	Percent of increase(%)
0.05	0.516	11.132	0.587	0.574	2.297
0.1	0.557	1.526	0.582	0.565	2.835
0.5	0.333	8.245	0.314	0.306	2.547
1	0.178	8.707	0.165	0.162	1.515
1.5	0.117	8.119	0.108	0.107	0.921
2	0.086	7.407	0.081	0.080	1.477

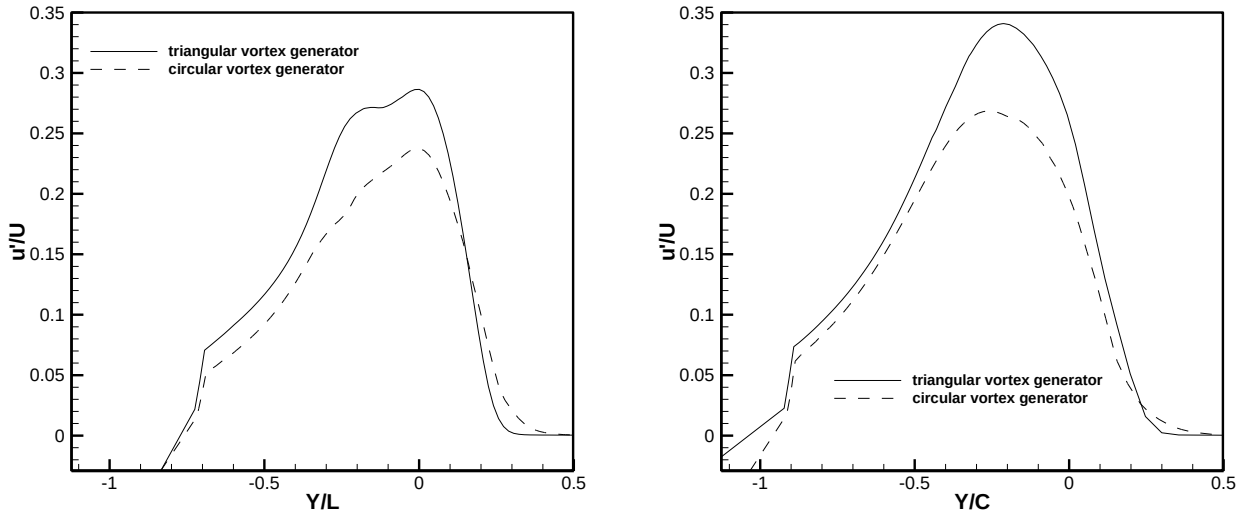

(a) (b)

Fig. 5. Reynolds stress at X/L: 0.5(a) & 1(b) behind vortex generator

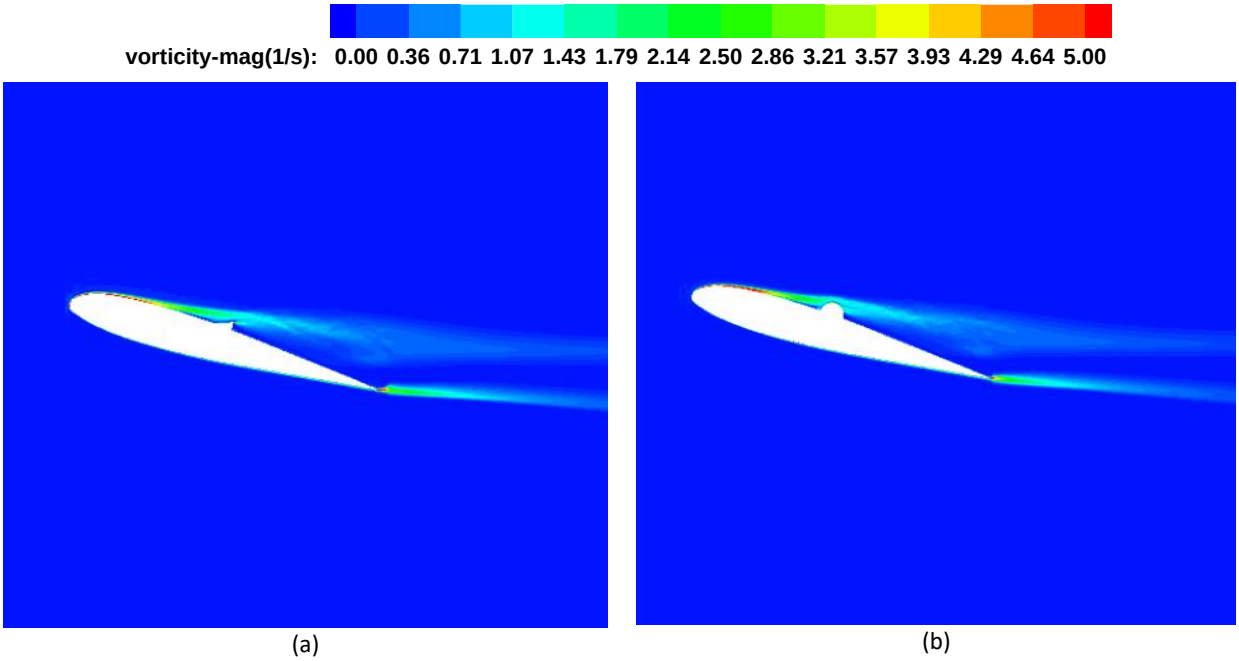

(a) (b)

Fig. 6. Vorticity magnitude behind triangular(a) and circular(b) vortex generator

3.3 Mean Velocity

In this section, the mean velocity profiles of B-737 airfoils with and without triangular and circular vortex generators are considered. Figure 7 shows the comparison of the mean velocity profile at station X/C=0.5, 1, 1.5, and 2. Just behind the airfoil, the velocity profiles have a sharper peak than the other stations which becomes more gradual as it gets farther from the trailing edge of the airfoil peaks. Figure 7 also shows the existence of the asymmetric shape of the airfoil with the top camber. So that the positive values of Y/C (top surface) reach the lower value of U/U0 than the negative Y/C (lower surface). As the vortex generators operate as an obstacle in the airflow direction, they take

part in decreasing the mean velocity behind the airfoil. So the mean velocity behind an airfoil with a circular vortex generator, due to its shape, is lower than airfoils with a triangular vortex generator and both of them are lower than simple airfoil without a vortex generator. The results show that as the stations get farther from the trailing edge, the wake of the airfoil is dissipated and the minimum of profile gets closer to unity. The minimum velocity is located in the centerline along the trailing edge. Figure 8 shows the velocity defect at each station predicted by the numerical solution for three cases of the airfoil. According to Figure 8, by getting farther from the trailing edge, the minimum of the velocity profiles gets closer to the free stream value. Another interesting result is that by getting farther from the trailing edge, the minimum values of the profiles for an airfoil with triangular vortex generators and simple ones get closer to each other and can be equal.

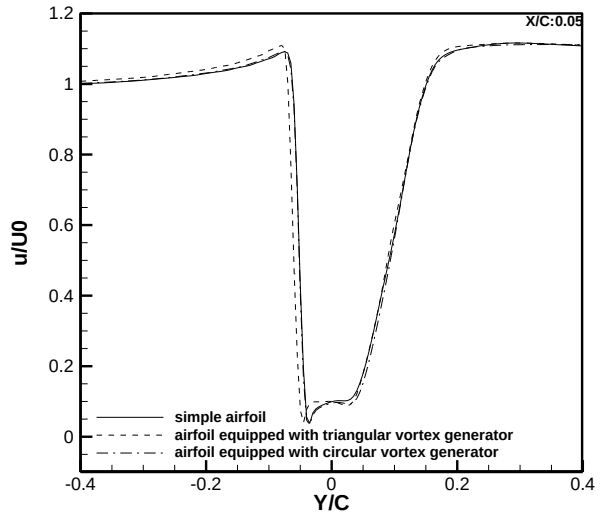

(a)

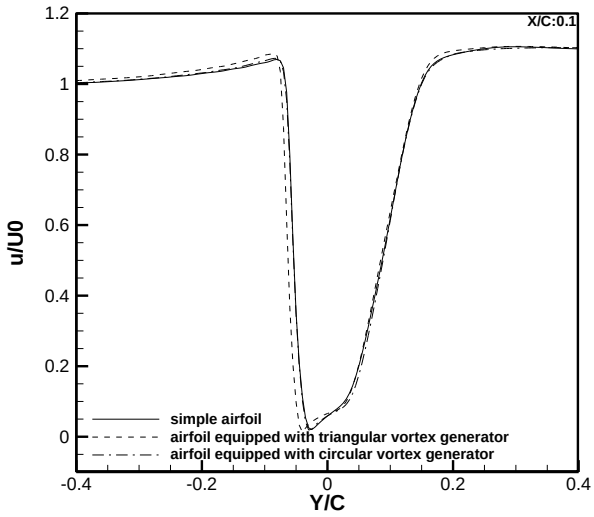

(b)

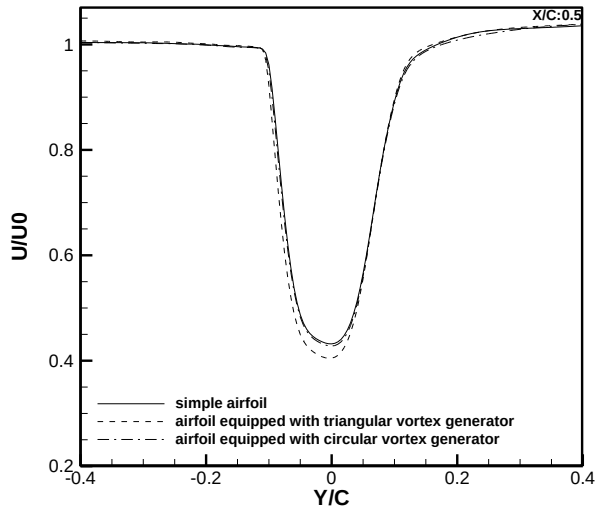

(c)

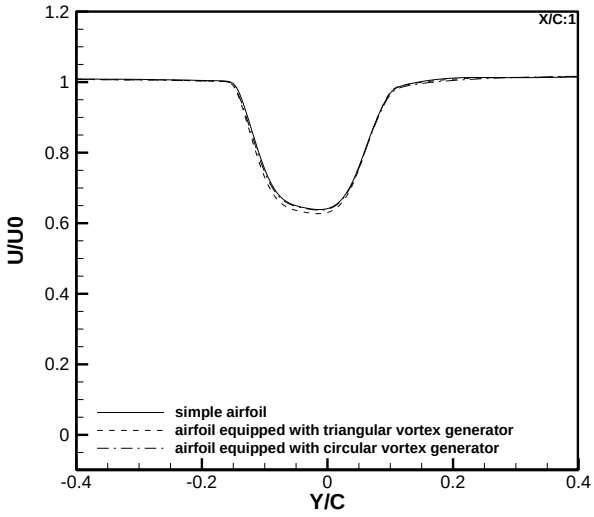

(d)

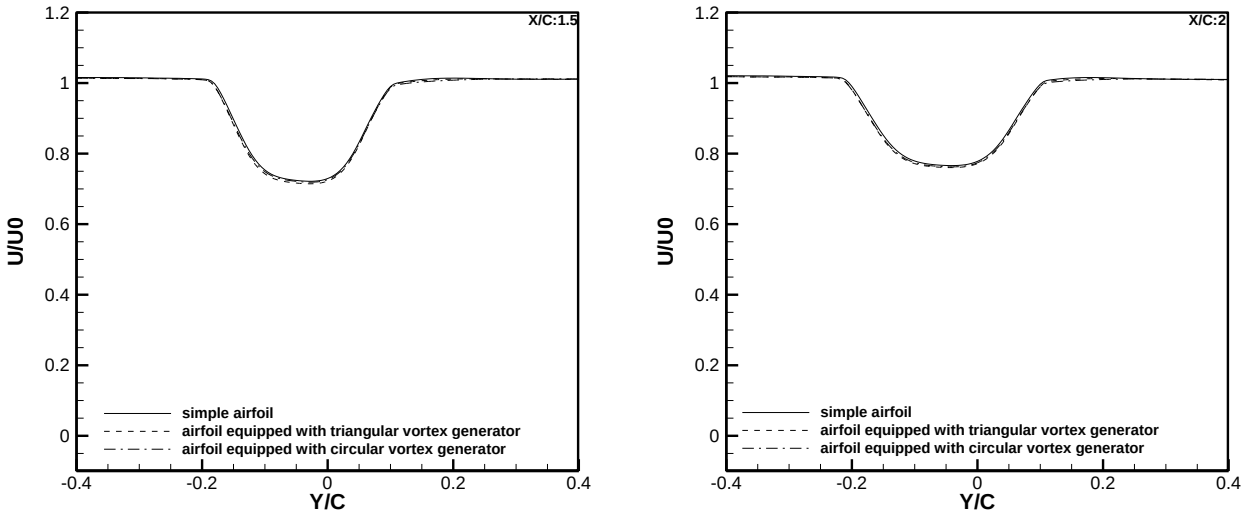

(e) (f)

Fig. 7. The comparison of mean velocity by RSM at stations X/C=0.05(a), 0.1(b), 0.5(c), 1(d), 1.5(e), 2(f)

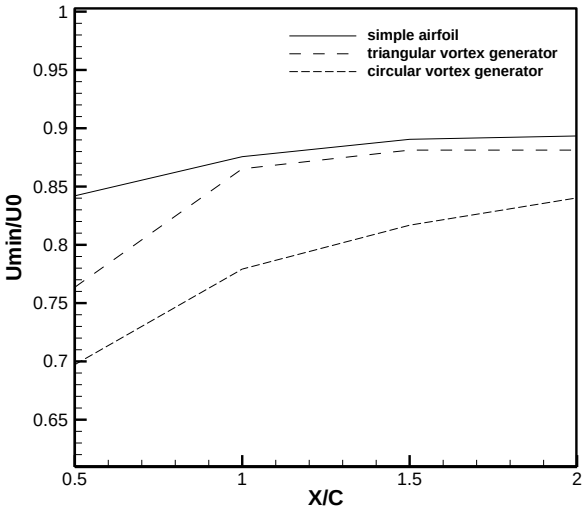

Fig. 8. Velocity defect at each station for simple, triangular, circular vortex generators equipped airfoils by RSM

3.4 Drag Force and Lift to Drag Ratio

In this section ,the effects of the presence of vortex generator on pressure drag, friction drag, total drag, drag coefficient and lift to drag ratio based on the obtained results are discussed. Vortex generators produce numerous small and large vorticities. These vorticities maintain the boundary layer attached to the surface. Conclusively, the separation of the boundary layer is postponed and maybe it doesn't even occur. For 0 angle of attack, the use of vortex generators increases the

pressure drag, while it decreases the lift to drag ratio significantly. The increase of pressure drag is 85.540% and 84.210% for triangular and circular vortex generators, respectively. At 0 angle of attack, the circular vortex generator produces less drag than the triangular vortex generator. The lift to drag ratio is decreased by 7070% and 2013.430% for triangular and circular vortex generators, respectively. By using the vortex generators at 15 degrees of angle of attack, when separation may occur, pressure drag decreases substantially, and due to the attached material the friction drag increases. The total drag decreases due to the dominant decrease in pressure drag. The drag coefficient also decreases. Table 4 shows the total drag compression of simple airfoil and vortex generator-equipped airfoils. Table 4 also shows the comparison of total drag, drag coefficient, and also lift to drag ratio of simple and vortex generator-equipped airfoils. According to table 4, by attaching the vortex generators to the bare airfoil, the drag coefficient is reduced by 0.161% and 0.806% for triangular and circular vortex generators, respectively. The lift to drag ratio is increased by 3.540% and 3.650% for triangular and circular vortex generators, respectively.

Table 4
Comparison of drag, drag coefficient and lift to drag ratio of airfoils

Airfoil type	Pressure drag(N)	Friction drag	Total drag(N)	C_d	L/D
Simple B-737(AOA:0)	69.666	50.801	120.468	0.983	14.160
Simple B-737(AOA:15)	1104.904	34.120	1139.025	9.389	12.620
B-737 with Triangular vortex generator(AOA:0)	481.898	37.461	519.360	4.239	0.020
B-737 with Triangular vortex generator(AOA:15)	1102.217	35.537	1137.755	9.285	13.080
B-737 with Circular vortex generator(AOA:0)	441.246	36.971	478.217	3.903	0.670
B-737 with Circular vortex generator(AOA:15)	1096.023	34.391	1130.415	9.225	13.100

4. Conclusion

In this study, the simple and vortex generator-equipped airfoils are studied by RSM. The results show that by getting farther from the trailing edge, the mean velocity decreases for all airfoil shapes. A study of Reynolds stress by the RSM model shows that the simple airfoil has two separated peaks of Reynolds stress versus the Y/C graph. Due to the asymmetry of the airfoil, the right peak (on the top surface) is usually higher than the left peak (bottom surface). The results also show that the vorticities of a circular vortex generator are stronger than the triangular vortex generator due to the separation of flow on a circular vortex generator. Just behind the airfoil, the velocity profiles have a sharper peak than the other stations which become more gradual as they get farther from the trailing edge of the airfoil peaks. As the vortex generators operate as an obstacle in the airflow direction, they take part in decreasing the mean velocity behind the airfoil. So the mean velocity behind an airfoil with a circular vortex generator, due to its shape, is lower than airfoils with a triangular vortex

generator. Also, both of them are lower than simple airfoil. The results show that as the stations get farther from the trailing edge, the wake of the airfoil is dissipated and the minimum of profiles gets closer to unity. The effects of the presence of vortex generator on pressure drag, friction drag, total drag, drag coefficient and lift to drag ratio are considered. The increase of pressure drag is 85.540% and 84.210% for triangular and circular vortex generators respectively at 0 AOA. At 0 angle of attack, the circular vortex generator produces less drag than the triangular vortex generator. The lift to drag ratio also is decreased by 7070% and 2013.430 for triangular and circular vortex generators, respectively. At 15 degrees of AOA, the total drag decreases due to the dominant decrease in pressure drag. By attaching the vortex generators to the simple airfoil, the drag coefficient is reduced by 0.161% and 0.806% for triangular and circular vortex generators, respectively. The lift to drag ratio is increased by 3.540% and 3.650% for triangular and circular vortex generators, respectively.

Acknowledgment
Thanks to the cooperation of Hakim Sabzevari University for assisting in this research.

References

[1] Bak Khoshnevis, Abdolamir, Shima Yazdani, and Erfan Salimipour. "Effects of CFJ flow control on aerodynamic performance of symmetric NACA airfoils." *Journal of Turbulence* 21, no. 12 (2020): 704-721.
[2] Farsimadan, E., and M. R. Mokhtarzadeh-Dehghan. "An experimental study of the turbulence quantities in the boundary layer and near-wake of an airfoil placed at upstream of a 90 bend." *Experimental thermal and fluid science* 34, no. 8 (2010): 979-991. https://doi.org/10.1016/j.expthermflusci.2010.02.005
[3] Jirasek, Adam, "Vortex-generator model and its application to flow control", *Journal of Aircraft* 42, no. 6 (2005): 1486-1491. https://doi.org/10.2514/1.12220
[4] Lei, Yonggang, Fang Zheng, Chongfang Song, and Yongkang Lyu. "Improving the thermal hydraulic performance of a circular tube by using punched delta-winglet vortex generators." *International Journal of Heat and Mass Transfer* 111, (2017): 299-311. https://doi.org/10.1016/j.ijheatmasstransfer.2017.03.101
[5] Lemenand, Thierry, Charbel Habchi, Dominique Della Valle, and Hassan Peerhossaini. "Vorticity and convective heat transfer downstream of a vortex generator." *International Journal of Thermal Sciences* 125, (2018): 342-349. https://doi.org/10.1016/j.ijthermalsci.2017.11.021
[6] Narasimhan, J. L., V. Ramjee, Philip M. Diwakar, and E. G. Tulapurkara. "Prediction of wake in a curved duct." *International journal for numerical methods in fluids* 13, no. 7 (1991): 907-916. https://doi.org/10.1002/fld.1650130708
[7] Okamoto, Shinsuke, Nobuhiro Homma, Akira Adachi, and Shinji Honami. "Dynamic Interaction of the Longitudinal Vortices by Active Vortex Generator." *In 3rd AIAA Flow Control Conference*, p. 3181. 2006. https://doi.org/10.2514/6.2006-3181
[8] Szwaba, Ryszard, Pawel Flaszynski, and Piotr Doerffer. "Streamwise vortex generation by the rod." *Chinese Journal of Aeronautics* 32, no. 8 (2019): 1903-1911. https://doi.org/10.1016/j.cja.2019.03.033
[9] Tulapurkara, E. G. "Turbulence models for the computation of flow past airplanes." *Progress in Aerospace Sciences* 33, no. 1-2 (1997): 71-165. https://doi.org/10.1016/S0376-0421(96)00002-4
[10] Tajuddin, Nurulhuda, Shabudin Mat, Mazuriah Said, and Shumaimi Mansor. "Flow characteristic of blunt-edged delta wing at high angle of attack." *Journal of Advanced Research in Fluid Mechanics and Thermal Sciences* 39, no. 1 (2017): 17-25.
[11] Adanta, Dendy, Budiarso Budiarso, Warjito Warjito, Ahmad Indra Siswantara, and Aji Putro Prakoso. "Performance comparison of NACA 6509 and 6712 on pico hydro type cross-flow turbine by numerical method." Journal of Advanced Research in Fluid Mechanics and Thermal Sciences 45, no. 1 (2018): 116-127.
[12] Adanta, Dendy, Budiarso Budiarso, and Ahmad Indra Siswantara. "Assessment of turbulence modelling for numerical simulations into pico hydro turbine." *Journal of Advanced Research in Fluid Mechanics and Thermal Sciences* 46, no. 1 (2018): 21-31.
[13] Hakim, Muhammad Syahmi Abdul, Mastura Ab Wahid, Norazila Othman, Shabudin Mat, Shuhaimi Mansor, Md Nizam Dahalan, and Wan Khairuddin Wan Ali. "The effects of Reynolds number on flow separation of Naca Aerofoil." *Journal of Advanced Research in Fluid Mechanics and Thermal Sciences* 47, no. 1 (2018): 56-68.

[14] Sajali, Muhammad Fahmi Mohd, Syed Ashfaq, Abdul Aabid, and Sher Afghan Khan. "Simulation of effect of various distances between front and rear body on drag of a non-circular cylinder." *Journal of Advanced Research in Fluid Mechanics and Thermal Sciences* 62, no. 1 (2019): 53-65.

[15] Tahseen, Tahseen Ahmad, Muhammad Asmail Eleiwi, and Ayad Fouad Hameed. "Numerical study of fluid flow and heat transfer in a backward facing step with three adiabatic circular cylinder." *Journal of Advanced Research in Fluid Mechanics and Thermal Sciences* 72, no. 1 (2020): 80-93.

[16] Cerutti, J. J., G. Cafiero, and G. Iuso. "Aerodynamic drag reduction by means of platooning configurations of light commercial vehicles: A flow field analysis." *International Journal of Heat and Fluid Flow* 90, (2021): 108823. https://doi.org/10.1016/j.ijheatfluidflow.2021.108823

[17] Li, Liang, Bin Zhou, Hongbo Huang, and Hongxing Sun. "Vortex generator design and numerical investigation for wake non-uniformity and cavitation fluctuation pressure reduction." *Ocean Engineering* 229, (2021): 108965. https://doi.org/10.1016/j.oceaneng.2021.108965

[18] Ricco, Pierre, Martin Skote, and Michael A. Leschziner. "A review of turbulent skin-friction drag reduction by near-wall transverse forcing." *Progress in Aerospace Sciences* 123, (2021): 100713. https://doi.org/10.1016/j.paerosci.2021.100713

[19] Nagler, Jacob. "On Boeing 737–300 wing aerodynamics calculations based on VLM theory." *Frontiers of Mechatronical Engineering* 1, (2018): 1-7. https://doi.org/10.18282/fme.v1i1.604

[20] KC, Real, Nicholas Lucido, Brian Elbing, Jamey Jacob, Aaron Alexander, Buddy Black, and Peter Ireland. "Study of Conformal Vortex Generators via Wake Survey." *Bulletin of the American Physical Society* 63, (2018) https://doi.org/10.2514/6.2019-0578

[21] Xue, Sidney, Bradley Johnson, David Chao, Ashish Sareen, and Carsten Westergaard. "Advanced aerodynamic modeling of vortex generators for wind turbine applications." *In European Wind Energy Conference (EWEC)*, Warsaw Poland. 2010

[22] Zhen, Tan Kar, Muhammed Zubair, and Kamarul Arifin Ahmad. "Experimental and numerical investigation of the effects of passive vortex generators on Aludra UAV performance." *Chinese Journal of Aeronautics* 24, no. 5 (2011): 577-583. https://doi.org/10.1016/S1000-9361(11)60067-8

[23] Anderson Jr, *JD (2010) Fundamentals of aerodynamics*. McGraw-Hill Education, New York